Data mining of petrophysical and lithogeochemical borehole data to elucidate the origin of seismic reflectivity within the Kevitsa Ni-Cu-PGE -bearing intrusion, northern Finland

Junno, Niina Marjut

2020-01-01

Junno , N M , Koivisto , E A-L , Kukkonen , I T , Malehmir , A , Wijns , C & Montonen , M 2020 , ' Data mining of petrophysical and lithogeochemical borehole data to elucidate the origin of seismic reflectivity within the Kevitsa Ni-Cu-PGE -bearing intrusion, northern Finland ' , Geophysical Prospecting , vol. 68 , no. 1 , pp. 82-102 . https://doi.org/10.1111/1365-2478.12907

http://hdl.handle.net/10138/310104
https://doi.org/10.1111/1365-2478.12907

Geophysical Prospecting

EAGE EUROPEAN ASSOCIATION OF GEOSCIENTISTS & ENGINEERS

Geophysical Prospecting, 2020, **68**, 82–102 doi: 10.1111/1365-2478.12907

Data mining of petrophysical and lithogeochemical borehole data to elucidate the origin of seismic reflectivity within the Kevitsa Ni–Cu–PGE bearing intrusion, northern Finland

N. Junno[1]*, E. Koivisto[1], I. Kukkonen[1], A. Malehmir[2], C. Wijns[3] and M. Montonen[4]

[1]*Department of Geosciences and Geography, University of Helsinki, Helsinki, PO. Box 68, FI-00014, Finland,* [2]*Department of Earth Sciences, Uppsala University, Uppsala, Sweden,* [3]*First Quantum Minerals Ltd., West Perth, WA 6005, Australia, and* [4]*Boliden FinnEx Oy, Kevitsa, Finland*

Received April 2019, revision accepted November 2019

ABSTRACT

The Kevitsa mafic-ultramafic intrusion, located within the Central Lapland Greenstone Belt in northern Finland, hosts a large, disseminated Ni–Cu–PGE sulphide deposit. A three-dimensional seismic reflection survey was conducted over the Kevitsa intrusion in 2010 primarily for open-pit mine planning and for deep mineral exploration purposes. In the Kevitsa three-dimensional seismic data, laterally continuous reflections are observed within a constrained region within the intrusion. In earlier studies, it has been suggested that this internal reflectivity mainly originates from contacts between the tops and more sulphide-rich bottoms of smaller scale, internally differentiated magma layers that represent a spectrum of olivine pyroxenites. However, this interpretation is not unequivocally supported by the borehole data. In this study, data mining, namely the Self-Organizing Map analysis, of extensive Kevitsa borehole data is used to investigate the possible causes for the observed internal reflectivity within the Kevitsa intrusion. Modelling of the effect of mineralization and alteration on the reflectivity properties of Kevitsa rock types, based on average modal compositions of the rock types, is presented to support the results of the Self-Organizing Map analysis. Based on the results, we suggest that the seismic reflectivity observed within the Kevitsa intrusion can possibly be attributed to alteration, and may also be linked to the presence of sulphide minerals.

Key words: Borehole geophysics, Petrophysics, Seismics, Interpretation.

1 INTRODUCTION

In the past decades, seismic reflection methods have increasingly been used for mining and mineral exploration applications in hard rock environments (Milkereit *et al.* 1996; Eaton, Milkereit and Salisbury 2003; Heinonen *et al.* 2012; review by Malehmir *et al.* 2012a; Buske, Bellefleur and Malehmir 2015 and references therein). In addition to their depth penetration, seismic reflection methods are of particular interest because of their significantly higher resolution when compared to other geophysical methods, and because petrophysical properties of sulphide minerals imply that sulphide deposits should generate strong seismic signals in typical hard rock environments (e.g. Salisbury, Harvey and Matthews 2003). The sulphide deposits could even directly be observed if they meet the size, thickness and geometrical constraints required for reflection or diffraction.

*E-mail: niina.junno@helsinki.fi

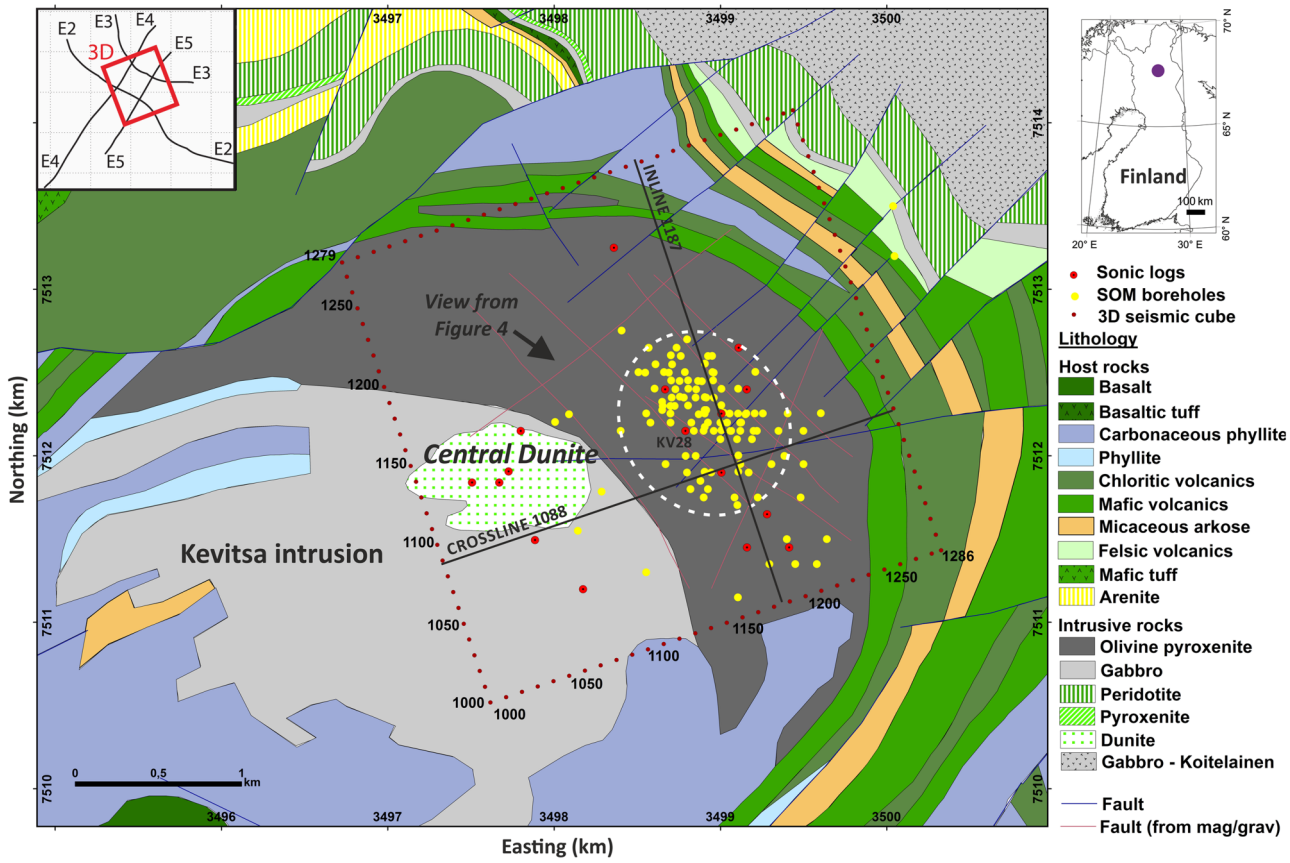

Figure 1 Geological map of the Kevitsa area. The Kevitsa intrusion mainly consists of olivine pyroxenites (dark grey) in the northeast and gabbros (light grey) in the southwest. A vast number of geological and geophysical data sets, in particular extensive borehole data and 3D seismic reflection data, are available from Kevitsa. The selected boreholes for the SOM analysis are presented on the geological map with yellow and red dots; red dots indicate boreholes containing sonic logs. The 3D seismic reflection survey area is indicated by a red dotted square, and it covers an area of about 9 km^2. The white dashed area represents the approximate area of the ultimate open-pit mine. Also shown is the location of the 3D seismic inline 1187 and crossline 1088 in Fig. 2. Inset map shows the location of earlier 2D seismic reflection lines relative to the 3D survey area. Bedrock geology has been modified from a map provided by First Quantum Minerals Ltd.

However, interpretation of seismic reflection data from hard rock mining and exploration environments is often challenging because of the geological complexity emanating from multiple phases of deformation and alteration that the rocks have experienced during their history (e.g. L'Heureux, Milkereit and Vasudevan 2009). Available borehole data sets provide only localized characterizations of the subsurface and are typically multiplex from the point of view of interpreting the causes of seismic anomalies on a larger scale. In recent years, data mining approaches have been used in growing numbers for data-driven analyses of the complex geophysical and geological data sets typical for mining and exploration camps (e.g. Klose 2006; Bierlein *et al.* 2008; Steel 2011; Cracknell, Reading and McNeill 2014; Kieu, Kepic and Kitzig 2018; Horrocks 2019), but examples on the use of data mining techniques for the interpretation of seismic data in hard rock settings are still lacking.

We use Self-Organizing Map (SOM; Kohonen 1981, 2001; Fraser and Dickson 2007) analysis to examine borehole data for the causes of seismic reflections within the Kevitsa intrusion. An SOM is a type of an artificial neural network and works on a vector quantization methodology that allows unsupervised analysis to identify the underlying linear and non-linear relationships between different data variables. Unsupervised analysis is preferable when there are no clear, previously established relationships between the data variables, for example between alteration and reflectivity properties, as is the case with the Kevitsa borehole data.

The Kevitsa mafic-ultramafic intrusion in northern Finland hosts a large, disseminated Ni–Cu–PGE sulphide deposit

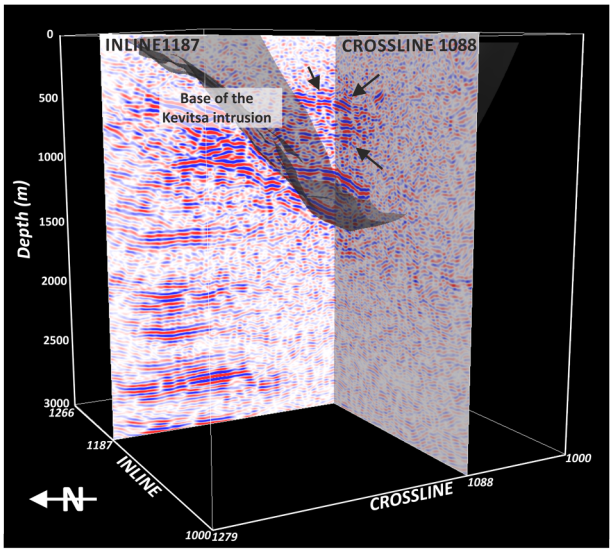

Figure 2 3D seismic reflection cube within the Kevitsa intrusion, viewed from the northeast: inline 1187 and crossline 1088 (migrated; Malehmir *et al.* 2012b) with reflections indicated by black arrows. The base of the Kevitsa intrusion from Koivisto *et al.* (2015) is shown in light grey as a reference.

(Fig. 1). Four intersecting two-dimensional seismic reflection profiles were acquired at Kevitsa in 2007 as part of the HIRE project (High-Resolution Reflection Seismics for Ore Exploration 2007–2010) to test the applicability of seismic surveying for exploration (Kukkonen, Lahti and Heikkinen 2009; Koivisto *et al.* 2012). In addition to the two-dimensional survey, a three-dimensional seismic reflection survey (see details from Malehmir *et al.* 2012b) was conducted in 2010, primarily for mine planning (Malehmir *et al.* 2012b; Koivisto *et al.* 2015; Lindqvist *et al.* 2017; Malehmir *et al.* 2017), but also for deep mineral exploration purposes (Malehmir *et al.* 2012b; Malehmir *et al.* 2014; Koivisto *et al.* 2015; Malehmir *et al.* 2017). In the seismic data, laterally continuous reflections were observed within a constrained region around the Kevitsa disseminated sulphide mineralization, from about 300 m to about 1 km depth (Fig. 2). These reflections were initially interpreted to originate from contacts between the tops and bottoms of smaller scale, internally differentiated olivine pyroxenite magma layers (Koivisto *et al.* 2012; Malehmir *et al.* 2012b; Malehmir *et al.* 2014; Koivisto *et al.* 2015). The magmatic layers were inferred to control the extent of the economic mineralization, with sulphides concentrated at the bottoms of the layers (Standing *et al.* 2009; Gregory *et al.* 2011). However, Koivisto *et al.* (2015) noted that while the acoustic impedance contrast between the suggested tops and bottoms of the magmatic layers seemed to be enough to produce detectable reflections, this explanation for the internal seismic reflectivity was not unequivocally supported by the borehole data as only little plagioclase-bearing olivine websterite, constituting the tops of the previously described magma layers, had been logged within the Kevitsa resource area (Gregory *et al.* 2011). Plagioclase-bearing olivine websterite has been logged only for 38 boreholes out of 871 boreholes available in the database provided by the mining company. The lack of plagioclase-bearing olivine websterite was tentatively attributed to varying historical logging practices that might not have correctly identified all the variants of olivine pyroxenites prior to a re-logging campaign that recognized the possible role of the magmatic layering in 2009 (Gregory *et al.* 2011). However, more recent geological works by Le Vaillant *et al.* (2016) and Luolavirta *et al.* (2018a,b) do not support such continuous layering but interpret the resource area to be associated with a local development of cyclic units, generally lacking obvious internal layering. Thus, the question arises as to what factors, other than mineralogical variations related to continuous smaller-scale magma layers, may explain the internal seismic reflectivity. In particular, the effect of alteration on the reflectivity properties has remained an open question (e.g. Koivisto *et al.* 2015).

The Kevitsa intrusion has gone through multiple alteration cycles resulting in widespread but varying alteration zones within the intrusion (Le Vaillant *et al.* 2016). However, in the borehole data, alteration is inadequately logged by varying practices over the years. For example, alteration is partly, but not consistently, indicated by a 'metaperidotite' label in the lithology rather than the alteration field. Metaperidotite refers to various degrees of amphibole alteration of olivine pyroxenites. The primary lithology, which has not been logged, may be olivine pyroxenite, olivine websterite, websterite or plagioclase-bearing olivine websterite, and the alteration may range from non-pervasive to pervasive. This masks the identification of the specific rock type as well as the degree of alteration. Separate alteration logs are available for some boreholes, but not consistently for all the data.

We use SOM analysis of Kevitsa borehole data to better understand the origin of the reflectivity within the Kevitsa intrusion, and its relationship with the lithological variation, alteration, and disseminated sulphide mineralization. First, theoretical calculations (Abers and Hacker 2016) are presented to provide insights into the effect of sulphide mineralization and alteration on the reflectivity properties of the Kevitsa rock types in order to support the interpretation of the SOM results. Then, we present SOM analysis of the borehole

data using different geophysical, geotechnical and geochemical data. Based on the results, we conclude that the seismic reflectivity observed within the Kevitsa intrusion can possibly be attributed to alteration, and may also be linked to the presence of sulphide minerals, rather than to primary lithological contacts between the tops and bottoms of smaller scale magma layers within the intrusion. Additionally, fracture and fault zones, rock fragments (dunite, host rocks, etc.), as well as dykes and veins internal to the Kevitsa intrusion could be potential reflectors if they meet the geometrical requirements for observable reflections.

2 GEOLOGICAL BACKGROUND

The Kevitsa intrusion and deposit are described in detail by Mutanen (1997) and Mutanen and Huhma (2001). The intrusion is located within the Central Lapland Greenstone Belt (CLGB) in northern Finland (Fig. 1). The CLGB rocks are mainly layered volcanic and sedimentary rocks of Palaeoproterozoic age. These volcano-sedimentary rocks and the Kevitsa intrusion were metamorphosed and hydrothermally altered during a regional greenschist facies metamorphic event (Mutanen 1997). The southwest dipping intrusion, dated at about 2.06 Ga (Mutanen 1997; Mutanen and Huhma 2001), consists of gabbroic rocks in the southwest and mafic-ultramafic olivine pyroxenite and its variations in the northeast. Several (probably) older dunite units, which may have played a role in the larger scale emplacement of the Kevitsa intrusion and possibly also in the formation of the disseminated mineralization (e.g. Luolavirta *et al.* 2018c), are found within and around the intrusion (e.g. Central Dunite in Fig. 1). The intrusion covers an area of about 16 km^2 on the surface (Mutanen 1997), and it reaches a depth of about 1.5 km at its deepest parts (Koivisto *et al.* 2012; 2015). The economic mineralization occurs in compositionally heterogeneous olivine pyroxenites (more about this below), whereas more homogeneous olivine pyroxenites occur outside the Kevitsa resource area.

Open-pit mining, with a planned final pit depth of about 550 m, commenced in 2012 by First Quantum Minerals Ltd. As of June 2016, Boliden operates the mine. The total mineral resource of Kevitsa is about 160 million tons with a cutoff of 0.16% Ni (Kokko 2018). At the current mining rate of about 8 million tons of ore per year, the expected life of mine is until 2032 (Kokko 2018).

Several different ore types have been identified (Mutanen 1997; Gregory *et al.* 2011; Santaguida *et al.* 2015; Luolavirta *et al.* 2018a,b). A southwest-dipping ore zone averaging 0.30% Ni and 0.41% Cu – the so-called regular ore – occurs as a layered series of a couple of tens of meters thick bodies, extending up to hundreds of meters, consisting of 2–6% disseminated sulphide minerals; mostly pyrrhotite, pentlandite and chalcopyrite, and several platinum group minerals with lesser economic contribution (Gregory *et al.* 2011). The average PGE grades of the regular ore are 0.21 ppm Pt, 0.15 ppm Pd and 0.11 ppm Au (Gregory *et al.* 2011). In addition to the regular ore, north plunging high-grade Ni–PGE mineralization has been identified. These high-grade Ni–PGE ore zones are discordant to the regular ore. They are generally considered to have formed separately, but the origin continues to be debated (Mutanen 1997; Yang *et al.* 2014; Santaguida *et al.* 2015). The high Ni–PGE mineralization occurs as small, discontinuous, lens like bodies that have thicknesses of a few to tens of meters. The overall sulphide content is similar to the regular ore, but the main sulphide minerals present are pentlandite, pyrite, millerite and heazlewoodite (Yang *et al.* 2014; Le Vaillant *et al.* 2016). This mineralization has higher and more variable nickel content, with Ni tenor greater than 10% (Santaguida *et al.* 2015), and lower copper content than the regular ore, and it contains more PGEs. The regular ore comprises the most important economic resource in Kevitsa, whereas the high Ni–PGE mineralization is volumetrically less significant (Gregory *et al.* 2011; Luolavirta *et al.* 2018a). In addition, a transitional ore type between the regular and high Ni–PGE ores has been identified (Mutanen 1997). Contact-type sulphide mineralization, possibly representing remobilization (Gregory *et al.* 2011), is intersected by a few boreholes that reveal Cu- and Ni-poor semi-massive to massive sulphides, which occur at or below the basal contact of the intrusion. Finally, the so-called 'false ore' (Mutanen 1997) refers to uneconomic iron sulphide minerals, almost entirely pyrrhotite, with very low Ni (Ni tenor of only 2–3%) and Cu concentrations (e.g. Santaguida *et al.* 2015; Le Vaillant *et al.* 2016). It occurs mainly at the margins of the intrusion.

After re-logging of selected boreholes in 2009, Standing *et al.* (2009) and Gregory *et al.* (2011) suggested that the extent of the main economic high-Cu mineralization (i.e. the regular ore) is controlled by the extent of smaller scale, laterally discontinuous, and internally differentiated olivine pyroxenite layers (Fig. 3a). The thicknesses of these individual magma layers were interpreted to be tens to hundreds of meters, within a restricted area inside the Kevitsa intrusive complex (Standing *et al.* 2009). The magma layers were suggested to represent a spectrum of olivine pyroxenites (Fig. 3b) ranging from plagioclase and orthopyroxene-rich tops (plagioclase-bearing olivine websterite) to increasing percentages of olivine and clinopyroxene (olivine pyroxenite) towards the bottoms of the layers.

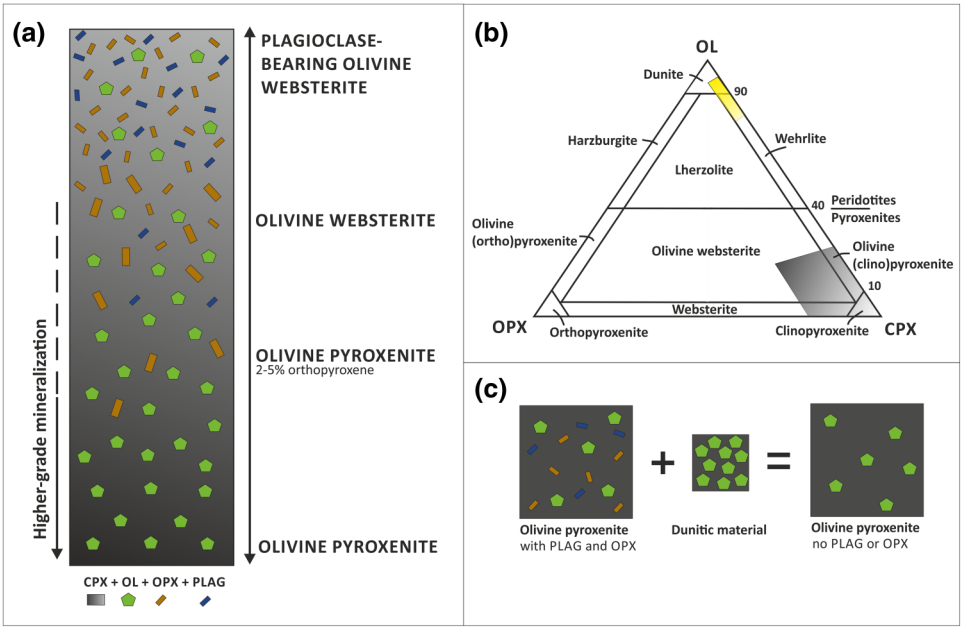

Figure 3 (a) Schematic drawing showing the mineralogical trends in the differentiated olivine pyroxenite magma layers, as suggested by Standing *et al.* (2009) (modified from Standing *et al.* 2009 and Gregory *et al.* 2011). Plagioclase (PLAG) and orthopyroxene (OPX) are more abundant at the top whereas olivine (OL) and clinopyroxene (CPX) are present throughout the layer, but dominate at the bottom. The mineralogical changes are gradational, that is, no hard boundaries exist within an individual magma layer. The sulphide mineralization grade gets higher towards the bottoms of the magma layers. (b) IUGS classification for ultramafic intrusive rocks (modified from Gregory *et al.* 2011): transparent grey area covers the general olivine pyroxenite variants in the Kevitsa resource area, whereas the transparent yellow area shows the approximate location of the north-plunging dunite intrusive. (c) Schematic drawing of the contamination of dunitic material (e.g. Standing *et al.* 2009) where plagioclase and orthopyroxene are replaced with olivine and clinopyroxene, hence resulting in magmas richer in olivine pyroxenite.

In the Kevitsa area, olivine clinopyroxenites are also called olivine pyroxenites (Standing *et al.* 2009). In addition, the orthopyroxene threshold for classification as olivine websterite was lifted from 10% orthopyroxene to 20%, in order to separate out the most distinctive rocks from the background, which generally contains 5–15% orthopyroxene. Olivine websterite is called 'plagioclase-bearing olivine websterite' where there is more than 5% plagioclase. The mineralogical change was interpreted to be gradational within an individual layer, with olivine websterite in the middle of the layers, and no internal contacts within the layers. However, the base of one layer (olivine pyroxenite) was described to grade relatively sharply to the top of another layer (plagioclase-bearing olivine websterite). The mineralization was suggested to be more strongly associated with the bases of these individual magma layers. However, this interpretation was not unambiguously supported by the borehole data, with only a handful of samples logged as plagioclase-bearing olivine websterite (Gregory *et al.* 2011; Koivisto *et al.* 2015). Recently, Le Vaillant *et al.* (2016) interpreted the ultramafic unit as composed of interlayered olivine pyroxenite and websterite with a local development of cyclic units, but for the most part lacking obvious internal layering. Luolavirta *et al.* (2018a) state that the overall internal architecture of the ultramafic unit is complex and dominated by relatively uniform olivine pyroxenites ranging in modal mineralogy from olivine clinopyroxenite to olivine websterite with local (i.e. only within the ore domain) discontinuous zones of plagioclase-bearing olivine websterite, but lacking obvious internal layering.

It has also been suggested that the dunite units within and around the Kevitsa intrusion have played a role in the genesis of the economic mineralization (e.g. Standing *et al.* 2009; Gregory *et al.* 2011; Luolavirta *et al.* 2018c). The Kevitsa intrusion is associated with a large dunitic body, called the Central Dunite (Fig. 1), with an overall discordant relationship to the Kevitsa intrusion (Koivisto *et al.* 2015; Luolavirta *et al.* 2018c). The Footwall Dunite forms a lens like body at the basal contact of the intrusion. Recent studies by Koivisto *et al.* (2015) and Luolavirta *et al.* (2018c) suggest a link between the Footwall Dunite and the Central Dunite that could indicate a shared origin of these two units. Additionally, dunitic and related ultramafic rocks occur as numerous

inclusions within the Kevitsa intrusion, being most common within the resource area. The dunite occasionally contains disseminated sulphides. Standing *et al.* (2009) proposed that contamination by dunitic material took place when the main Kevitsa magma intruded, and that this contamination may also mask magmatic layering. Mixing of dunitic material with the plagioclase and orthopyroxene-rich tops of the magma layers would result in more olivine and clinopyroxene-rich magmas, similar to the previously described bottoms of the magma layers (Fig. 3c).

Three main alteration styles have been identified within the Kevitsa intrusion: (1) a widespread amphibole alteration, consisting of replacement of clinopyroxene and orthopyroxene by tremolite-actinolite and cummingtonite-grunerite, respectively; (2) a pervasive, partial serpentinite alteration of olivine in peridotitic rocks; and (3) a structurally controlled epidote alteration associated with NE-trending faults cutting across the deposit (Le Vaillant *et al.* 2016). The serpentine alteration appears to be the first alteration event in Kevitsa, followed by amphibole alteration, and lastly epidote alteration (e.g. Standing *et al.* 2009). The epidote alteration style is concentrated within the NE-trending fault zones towards the south end of the ore body, whereas the amphibole and serpentinite alteration styles are spread throughout the intrusion, and enclose decimetre-scale patches of essentially fresh igneous rock. Alteration of pyroxenes and olivine is intense in places, making primary rock types difficult to identify. In the borehole data, the detailed distribution of the alteration is difficult to assess, and has been recorded with varying practices over the years, but the most intense zones appear to be directly associated with relatively late mafic dikes and veins (Santaguida *et al.* 2015; Le Vaillant *et al.* 2016). Large amphibole alteration zones containing closely spaced carbonate and carbonate-quartz veins are common throughout the intrusion; the veins are intimately associated with the alteration (Le Vaillant *et al.* 2016). It is thought that the alteration processes did not affect the Ni and PGE grades (Santaguida *et al.* 2015; Le Vaillant *et al.* 2016). Nevertheless, Le Vaillant *et al.* (2016) suggest that Cu and Au grades may have been affected by remobilization from centimetre to kilometre scale.

3 PHYSICAL ROCK PROPERTIES

Kevitsa has been the target of extensive geological and geophysical investigations since its discovery in 1987. A vast number of geophysical and geological data sets, including extensive borehole data and two-dimensional and three-dimensional (3D) seismic reflection data, are available. We have access to about 900 boreholes drilled within the Kevitsa resource area and its surroundings. However, about 70% of the boreholes are less than 300 m deep, and only 134 boreholes contain geophysical logs. Furthermore, sonic logs are only available from 16 boreholes.

In Fig. 4, the average P-wave velocities are plotted against average densities for the main lithologies observed in the Kevitsa borehole data (values listed in Table 1). The highest velocities and densities are associated with olivine websterite and olivine pyroxenite. The corresponding rock types with lesser amounts of olivine – websterite and pyroxenite – have lower seismic velocities and densities. The presence of plagioclase also decreases the seismic velocity and density. The peridotitic rocks in Kevitsa have undergone pervasive serpentinization of the olivine minerals (e.g. the Central Dunite). Serpentine has lower seismic velocity and density than olivine (e.g. Table 2; Bass 1995; Abers and Hacker 2016) and thus serpentinization lowers seismic velocity and density of the rocks (e.g. the difference between dunite and Central Dunite, in Fig. 4a, the latter of which is thoroughly serpentinized). Widespread amphibole alteration has taken place within the whole intrusion. Amphibole has lower seismic velocity and density than pyroxene (e.g. Table 2; Bass 1995; Abers and Hacker 2016) and, therefore, this replacement of pyroxenes with amphiboles also reduces seismic velocity and density of the Kevitsa rock types (e.g. change from olivine pyroxenite to metaperidotite, which is partly, but not consistently, used to describe amphibole-altered olivine pyroxenites in the Kevitsa borehole data; Fig. 4a). Overall, the hosting Central Lapland Greenstone Belt rocks are associated with lower velocities and densities than the intrusive rocks. The lowest seismic velocities and densities are associated with fractured and sheared rocks.

Referring to the earlier studies associating reflectors with magmatic layering (e.g. Koivisto *et al.* 2012, Koivisto *et al.* 2015), Fig. 4(a) indicates that the contrast between the physical properties of plagioclase-bearing olivine websterite, the tops of the magma layers, and olivine pyroxenite, the bottoms, would be enough to produce detectable reflections. However, for interpreting 3D seismic reflection data, there is a challenge in comparing pointwise borehole data with continuous 3D seismic reflection data. In the case of Kevitsa, tying the borehole data to the seismic reflection data is further complicated by poor reflectivity at shallow depths due to the high background velocity of the Kevitsa intrusion (greater than 6500 m/s) and issues with the sampling of the seismic wavefield at shallow depths (and low seismic fold). Due to these issues the observed reflectivity starts from approximately 300 m depth (i.e. shallower reflectors are simply not imaged), and the

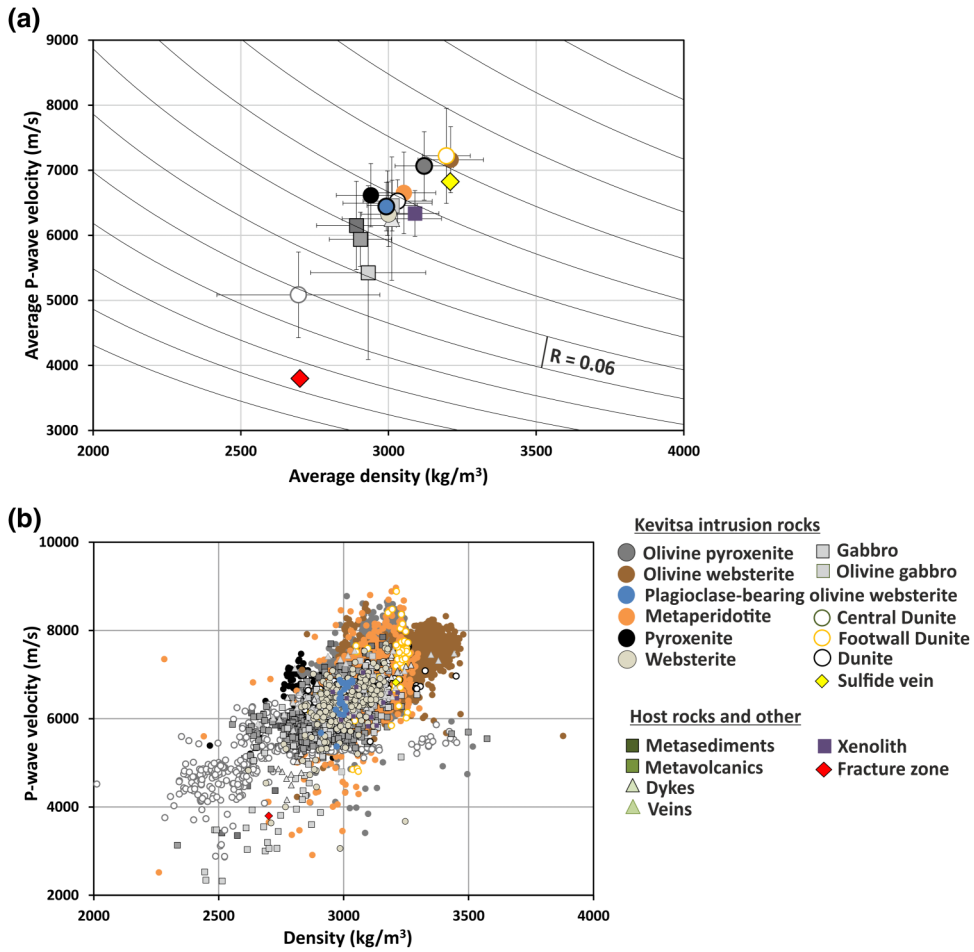

Figure 4 (a) Average P-wave velocity versus density plotted for the main lithologies observed in the Kevitsa borehole data (Table 1). Standard deviation is used for the error bars. The solid black curves correspond to constant acoustic impedance, and the difference between two curves represents a detectable reflection (reflection coefficient equals to 6%; Salisbury *et al.* 1996; Salisbury *et al.* 2003). There is sufficient contrast between the physical properties of plagioclase-bearing olivine websterite (blue dot) and olivine pyroxenite (grey dot), constituting the said tops and bottoms of suggested magma layers, to produce detectable reflections. (b) Overall distribution of density and P-wave velocity among different rock types in Kevitsa based on 15 boreholes. The figure has been modified from Koivisto *et al.* (2012) and does not include all the later boreholes included in this work.

laterally most continuous reflections start at depth of about 500 m (Fig. 2). Thus, the lack of borehole data at the depths of the reflections (only 61 boreholes out of 134 selected for the analysis are deeper than 500 m) limits the interpretation efforts.

3.1 Theoretical modelling of the effect of sulphide mineralization and alteration on the reflectivity properties of the Kevitsa rock types

In order to support the interpretation of the borehole data with regard to the reflectivity properties, we constructed forward models of the effect of sulphide mineralization and alteration on the densities and seismic P-wave velocities, that is on the seismic impedances of the Kevitsa rock types and ore. This helps overcome the inadequate and incomplete log data on the distribution of alteration within the intrusion. Alteration has been logged for only 41.5% of the samples chosen for the analysis, but an empty logging field for alteration indicates missing information and not necessarily lack of alteration. Exact quantitative modal compositions of Kevitsa lithologies are not available. Therefore, we calculated theoretical rock densities and velocities of the main rock types in Kevitsa using plausible modal compositions of the rock and ore types guided by the petrographic data provided by Mutanen (1997). Bulk rock properties were estimated using the

Table 1 Average P-wave velocities (*Vp*) and densities for the main lithologies and their standard deviations. The average acoustic impedance for each lithology group is also calculated. Originally, there were more than 70 different lithology labels used for the borehole data, but these were re-organized and simplified into 18 different classes listed here

Lithology Group Name	Average *Vp* (m/s)	Standard Deviation (m/s)	Average Density (kg/m^3)	Standard Deviation (kg/m^3)	Acoustic Impedance (10×10^6 kg/m^2/s)	No. of Samples
Olivine pyroxenite	7066	526	3121	99	22	3640
Olivine websterite	7161	508	3211	111	23	2917
Plagioclase-bearing olivine websterite	6441	373	2993	24	19	24
Metaperidotite	6652	627	3052	108	20	1696
Pyroxenite	6616	487	2940	117	19	243
Websterite	6324	613	3000	92	19	267
Central Dunite	5085	658	2695	276	14	363
Footwall Dunite	7222	731	3196	81	23	82
Dunite	6525	329	3031	117	20	183
Gabbro	5426	1335	2931	195	16	93
Olivine gabbro	6457	389	3012	85	19	44
Dyke	6256	948	3011	168	19	36
Vein	6493	496	2997	151	19	66
Metavolcanics	5938	416	2905	105	17	671
Metasediments	6151	678	2891	135	18	129
Xenolith	6336	352	3090	81	20	14
Fracture zone	7179	0	2626	0	19	1
Sulphide vein	6826	0	3209	0	22	1

Table 2 Theoretical densities and P-wave velocities for the most important rock and ore-forming minerals in Kevitsa (Bass 1995; Abers and Hacker 2016)

Mineral	Density (kg/m^3)	P-wave Velocity (m/s)	Notes
Pyrite	4910	7990	
Chalcopyrite	4280	5120	
Pyrrhotite	4710	4600	
Pentlandite	4680	4560	
Graphite	2226	11,650	
Magnetite	5202	7271	
Mg-Olivine (Forsterite)	3223	8585	
Fe-Olivine (Fayalite)	4401	6838	
Talc	2785	6533	
Chlorite	2636	6837	Mg-chlorite
Orthopyroxene	3197	8155	Enstatite
Clinopyroxene	3269	8104	
Hornblende	3183	6849	
Tremolite	2980	7164	
Serpentine	2586	6660	Antigorite
Ca-Plagioclase (Anorthite)	2761	6869	
Na-Plagioclase (Albite)	2621	6435	
Epidote	3348	8128	Zoisite
Carbonate	2861	7100	Dolomite
Sericite	2829	6203	Muscovite
Quartz	2650	6030	

geometric means of the mineral properties (shown in Table 2) weighted by the volume percentages of the minerals. The densities and seismic velocities were calculated for 0.03 GPa and 25°C (approximately corresponding to conditions in Kevitsa at 1 km depth) using the software and data by Abers and Hacker (2016) and Bass (1995). Porosity was assumed to be small and negligible.

The results of our theoretical modelling are shown in Fig. 5 and Table 3. Compositional trends related to alteration are shown as well as the effect of increasing sulphide mineral content. Alteration of olivine into serpentine, magnetite and carbonate was calculated assuming that in a thorough alteration of the mineral, the forsterite component has produced serpentine and the fayalite component has produced magnetite and carbonate. For the forsterite content, we applied a value of 85% (the range of values reported by Mutanen (1997) is about 77–90%). Amphibole alteration of pyroxenes was modelled assuming that the secondary amphibole consists of 50% hornblende and 50% tremolite (seismic velocity and density values are available for these; the properties should be close to tremolite-actinolite and cummingtonite-grunerite which are the alteration products of clinopyroxene and orthopyroxene, respectively). Properties of unaltered and altered plagioclase were calculated using an anorthite content of 80% (Mutanen 1997). Table 3 presents results for model

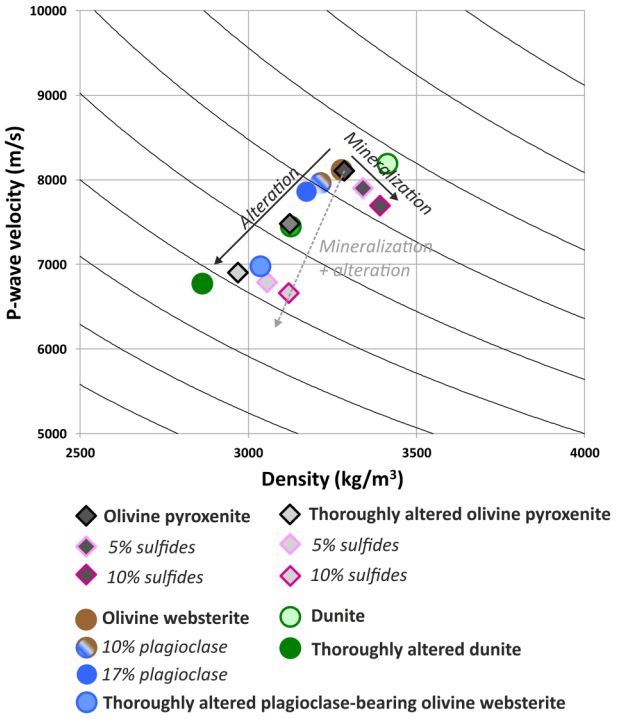

Figure 5 Theoretically calculated density and velocity values of Kevitsa rock types using a geometrical mean of the rock-forming minerals. The modal compositions are given in Table 3. Arrows indicate various trends due to alteration of olivine, pyroxenes and plagioclase, and mineralization. Effect of sulphide mineral content (0–10%) is shown with diamonds. The combined effect of sulphide mineralization and alteration is shown by the dashed grey arrow. The solid black curves correspond to constant acoustic impedance, and the difference between two curves should be enough for a detectable reflection (reflection coefficient equal to 6%; Salisbury *et al.* 1996; Salisbury *et al.* 2003).

compositions assuming fresh, altered (50%) and thoroughly altered (100%) compositions. The model compositions (Table 3) are not meant to be exact numerical representations of the results of complicated mineral reactions, but only to demonstrate the trends due to compositional variation and alteration.

Based on these results, it is obvious that unaltered rocks are not able to produce strong reflection contrasts. There is practically no impedance contrast between fresh variants of olivine pyroxenites (Fig. 5 and Table 3). Even adding 17% plagioclase to olivine websterite (in Kevitsa the plagioclase-bearing olivine websterite typically contains only 5–10% of plagioclase; Standing *et al.* 2009) is not enough to cause a reflection when in contact with olivine pyroxenite (i.e. this would be the contact between unaltered tops and bottoms of the magma layers as suggested by Standing *et al.* 2009). Furthermore, adding up to 10% sulphides (pyrrhotite, pentlandite and chalcopyrite) to olivine pyroxenite does not markedly change the impedance, although it will increase density. Such a volume of sulphides already exceeds the typical values in the Kevitsa ores (2-6%; Mutanen 1997). The same insensitivity to sulphide content applies to altered or thoroughly altered olivine pyroxenite. On the other hand, alteration is able to create a considerable shift in impedance against unaltered rock, which easily exceeds the detection threshold of a reflector (approximately 6% in reflection coefficient; Salisbury, Milkereit and Bleeker 1996; Salisbury *et al.* 2003).

Another immediate conclusion from the modelling is that the low sulphide mineral content cannot alone produce reflectivity of the Kevitsa ore. Although magnetite would have a strong (pyrite-like) effect on impedance, it is not present in sufficient amounts to make much of a difference, as can be seen, for instance, in the case of our modelled composition of a thoroughly altered dunite (containing 10% magnetite). On the other hand, alteration easily produces impedance contrasts creating reflection coefficients in the range of 10–15%.

4 METHOD AND DATA

4.1 Self-Organizing Map analysis

A Self-Organizing Map (SOM; Kohonen 1981, 2001) is a type of an unsupervised artificial neural network that is trained to produce a low-dimensional, discretized representation, typically a two-dimensional 'map', of complex high-dimensional input data. It differs from other artificial neural networks in that it applies competitive learning (vector quantization) as opposed to error-correction learning, and it uses a neighbourhood function to preserve topological relationships of the input data space. CSIRO's (Commonwealth Scientific and Industrial Research Organization) Self-Organizing Map software (Fraser and Dickson 2007), based on a Matlab SOM Toolbox (Kohonen *et al.* 1996; Vesanto *et al.* 2000), is used in this study.

SOM analysis has widely been used for applications ranging from engineering and oil industry to life sciences and finance (Kaski, Kangas and Kohonen 1998; Oja, Kaski and Kohonen 2003; Pöllä, Honkela and Kohonen 2009). Now, the SOM approach is making its way into hard rock mineral exploration (e.g. Klose 2006; Bierlein *et al.* 2008; Steel 2011; Cracknell *et al.* 2014; Leväniemi, Hulkki and Tiainen 2016). Major strengths of the technique comprise robust handling of multivariate, disparate and incomplete input data, including also categorical variables (e.g. Fessant and Midenet 2002;

Table 3 Modal mineral compositions, calculated densities and velocities of modelled rock types

Mineral	Unit	Unaltered Dunite	Altered Dunite	Thoroughly Altered Dunite	Unaltered Olivine-Pyroxenite	Altered Olivine-Pyroxenite	Thoroughly Altered Olivine-Pyroxenite	Unaltered Olivine-Pyroxenite with 5% Sulphides	Unaltered Olivine-Pyroxenite with 10% Sulphides	Unaltered Olivine-Pyroxenite with 20% Sulphides	Unaltered Olivine-Pyroxenite with 30% Sulphides	Unaltered Olivine-Websterite	Unaltered 10% Plg-Bearing Olivine-Websterite	Unaltered 17% Plg-Bearing Olivine-Websterite	Thoroughly Plg-Altered 17% Plg-Bearing Olivine-Websterite	Thoroughly Altered 17% Plg-Bearing Olivine-Websterite	Altered Olivine-Pyroxenite with 5% Sulphides	Thoroughly Altered Olivine-Pyroxenite with 5% Sulphides	Thoroughly Altered Olivine-Pyroxenite with 10% Sulphides	Thoroughly Altered Olivine-Pyroxenite with 10% Sulphides and 2% Graphite	Thoroughly Altered Olivine-Pyroxenite with 10% Sulphides and 10% Graphite	Thoroughly Altered Olivine-Pyroxenite with 20% Graphite
Chalcopyrite	v%	0	0	0	0	0	0	2	4.0	8.0	10.0	0	0	0	0	0	2.0	2.0	4.0	4.0	4.0	0
Pyrrhotite	v%	0	0	0	0	0	0	2	4	8	10	0	0	0	0	0	2.0	2.0	4.0	4.0	4.0	0
Pentlandite	v%	0	0	0	0	0	0	1.0	2.0	4.0	8.0	0	0	0	0	0	1.0	1.0	2.0	2.0	2.0	0
Quartz	v%	0	0	0	0	0	0	0	0	0	0	0	0	0	0	0	0	0	0	0	0	0
Fosterite	v%	72.0	36.0	0	7.0	3.5	0	6.6	6.5	5.8	5.3	8.0	6.4	5.9	5.9	0.0	3.5	0	0	0	0	0
Fayalite	v%	18.0	9.0	0	2.0	1.0	0	2.0	1.7	1.5	1.3	2.0	1.6	1.5	1.5	0	0.9	0	0	0	0	0
Talc	v%	0	5.0	10.0	0	0	0	0	0	0	0	0	0	0	0	0	0	0	0	0	0	0
Chlorite	v%	0	1.3	2.5	0	11.4	22.8	0	0	0	0	0	0	0	0	3.2	10.8	21.6	20.5	20.0	18.3	18.3
Orthopyroxene	v%	0	0	0	0	0	0	0	0	0	0	10.0	8.0	7.4	7.4	0	0	0	0	0	0	0
Clinopyroxene	v%	10.0	5.0	0	91.0	45.5	0	86.4	81.8	72.7	65.4	80.0	74.0	68.0	68.0	0	43.2	0	0	0	0	0
Hornblende	v%	0	2.5	5.0	0	22.8	45.5	0	0	0	0	0	0	0	0	37.7	21.6	43.2	40.9	40.0	36.5	36.5
Tremolite	v%	0	1.3	2.5	0	11.4	22.8	0	0	0	0	0	0	0	0	37.7	10.8	21.6	20.5	20.0	18.3	18.3
Serpentine	v%	0	30.0	60.0	0	4.0	8.0	0	0	0	0	0	0	0	0	3.2	3.3	6.6	6.2	6.0	5.0	5.0
Anorthite	v%	0	0	0	0	0	0	0	0	0	0	0	6.5	11.2	0	0	0	0	0	0	0	0
Albite	v%	0	0	0	0	0	0	0	0	0	0	0	3.5	6.1	5.8	5.8	0	0	0	0	0	0
Epidote	v%	0	0	0	0	0	0	0	0	0	0	0	0	0	5.8	5.8	0	0	0	0	0	0
Carbonate	v%	0	5.0	10.0	0	0	0	0	0	0	0	0	0	0	0	1.0	0	0	0	0	0	0
Sericite	v%	0	0	0	0	0	0	0	0	0	0	0	0	0	5.7	4.7	0	0	0	0	0	0
Graphite	v%	0	0	0	0	0	0	0	0	0	0	0	0	0	0	0	0	0	0	2.0	10.0	20.0
Magnetite	v%	0	5.0	10.0	0	0.5	1.0	0	0	0	0	0	0	0	0	1.0	1.0	2.0	2.0	2.0	2.0	2.0
Sum	v%	100	100	100	100	100	100	100	100	100	100	100	100	100	100	100	100	100	100	100	100	100
Bulk rock density	kg/m^3	3414	3126	2863	3285	3123	2969	3341	3392	3502	3596	3277	3215	3173	3214	3036	3194	3056	3120	3103	3035	2827
Bulk rock velocity	m/s	8193	7450	6775	8109	7483	6905	7904	7698	7302	6991	8119	7965	7863	7895	6980	7329	6792	6663	6734	7023	7675
Impedance	10^6 $kg/m^2/s$	27.55	23.12	19.40	26.60	23.35	20.50	26.36	26.06	25.54	25.11	26.56	25.68	25.05	25.30	21.19	23.39	20.75	20.79	20.90	21.32	21.70

Cottrell and Letrémy 2005). The SOM is robust in performing several operations, such as prediction, clustering, pattern recognition, and classification, on large volumes of data. Because SOM is unsupervised, no prior knowledge is needed of the nature or number of groupings within the data. Here, the principles of the SOM are briefly introduced. For further information, the reader is referred to Kohonen (1981, 2001), Vesanto *et al.* (2000) and Fraser and Dickson (2007).

An SOM consists of a predefined number of nodes that are organized on a typically two-dimensional, regularly spaced hexagonal or rectangular grid. The size of the SOM is equal to the number of nodes. These nodes are associated with *n*-dimensional (*n*D) vectors, where *n* is equal to the dimension of the input data vectors, that is the number of variables associated with the input data. Each node vector is connected to its neighbouring node vectors with a neighbourhood function that dictates the structure of the map. Often, a sheet map shape is used, but cylinder and toroid shapes can also be used.

In the SOM, each input data sample is treated as an *n*D data vector in a data space defined by its variables. The node vectors are trained in an iterative two-step learning process to represent the original distribution of the input data vectors. First, a random starting input data vector is selected and the similarity between it and all the node vectors of the SOM is measured using, typically, Euclidean distance. The node, which vector is the most similar, that is the closest, to the starting input data vector is called the Best Matching Unit (BMU). After finding the BMU, the node vectors are updated so that the BMU moves closer to the input data vector in the data space. Next, the neighbours of the BMU are also updated, but with lesser magnitude depending on the learning rate and distance from the BMU. The learning process is repeated several times for each input data vector while reducing learning rate and neighbourhood radius. The training is performed in two phases. At first, the learning rate and neighbourhood radius are initially set large (the neighbourhood radius should at the beginning cover the whole SOM map), and in the second phase they are set smaller. After training, the node vectors are situated within the original input data vectors. Each node vector represents a group or cluster of the data vectors closest to it, and if several node vectors are close together they can be subsets of a larger group or cluster. In the SOM, κ-means clustering is used. Davies–Bouldin (DB) analysis (Davies and Bouldin 1979) can be used to determine an appropriate number of clusters. Regression, a process that preserves the topology of the node vectors, is used to map the node vectors from *n*D space onto a two-dimensional (2D) map (each node on this 2D map represents a node vector in the *n*D space). The underlying statistical relationships between different data are visualized with the help of these 2D maps that facilitate the interpretation of the complex multidimensional data (e.g. Penn 2005; Fraser and Dickson 2007; Bierlein *et al.* 2008).

The quality of SOM is measured with two types of error calculations: quantization and topological error. The quantization error describes the map resolution; it measures the average distance between each input data vector and its BMU. The topological error measures the proportion of all data vectors for which first and second BMUs are not adjacent units (Vesanto *et al.* 2000).

The outputs of the SOM are shown in Fig. 6. The component plot (Fig. 6c) represents each node's contribution to a particular variable, with red colours indicating higher values of the variable and blue colours indicating smaller values of the variable. The unified distance matrix, or the U-matrix (Fig. 6d), represents the 2D topology of the SOM nodes, where the distance between neighbouring nodes is represented with different colours, blue representing shorter Euclidean distances (i.e. similarity) and red larger distances (i.e. difference). To aid the visualization of the distance between nodes, 'empty' nodes are added in between the actual nodes. White hexagons (Fig. 6d) represent the actual nodes. The number of original input data vectors that ultimately reside within each node is represented by the size of the white hexagon (e.g. Fraser and Dickson 2007).

4.2 The Kevitsa borehole data used in the SOM analysis

In total, 134 boreholes were selected for the Self-Organizing Map (SOM) analysis (Fig. 1). The selected boreholes contain data for at least one geophysical variable, are at least 300 m deep (the quality of the three-dimensional seismic data is very poor at shallower depths than 300 m) and are primarily located within the planned Kevitsa open pit area (indicated with a white dashed circle in Fig. 1). Exceptions were made for boreholes containing geophysical data, especially sonic logs.

Before the actual SOM analysis, the borehole data were re-sampled to uniform 1-m downhole intervals using a simple nearest neighbour interpolation method (data samples within 0.5 m from the depth location in question were considered), and anomalous data values (e.g. seismic velocities greater than 10,000 m/s) were removed.

Several tests were run to select representative geophysical, geotechnical and geochemical variables, and to perform preliminary data analyses on the selected variables. Junno *et al.* (2019) discuss how different sets of variables affect the ability

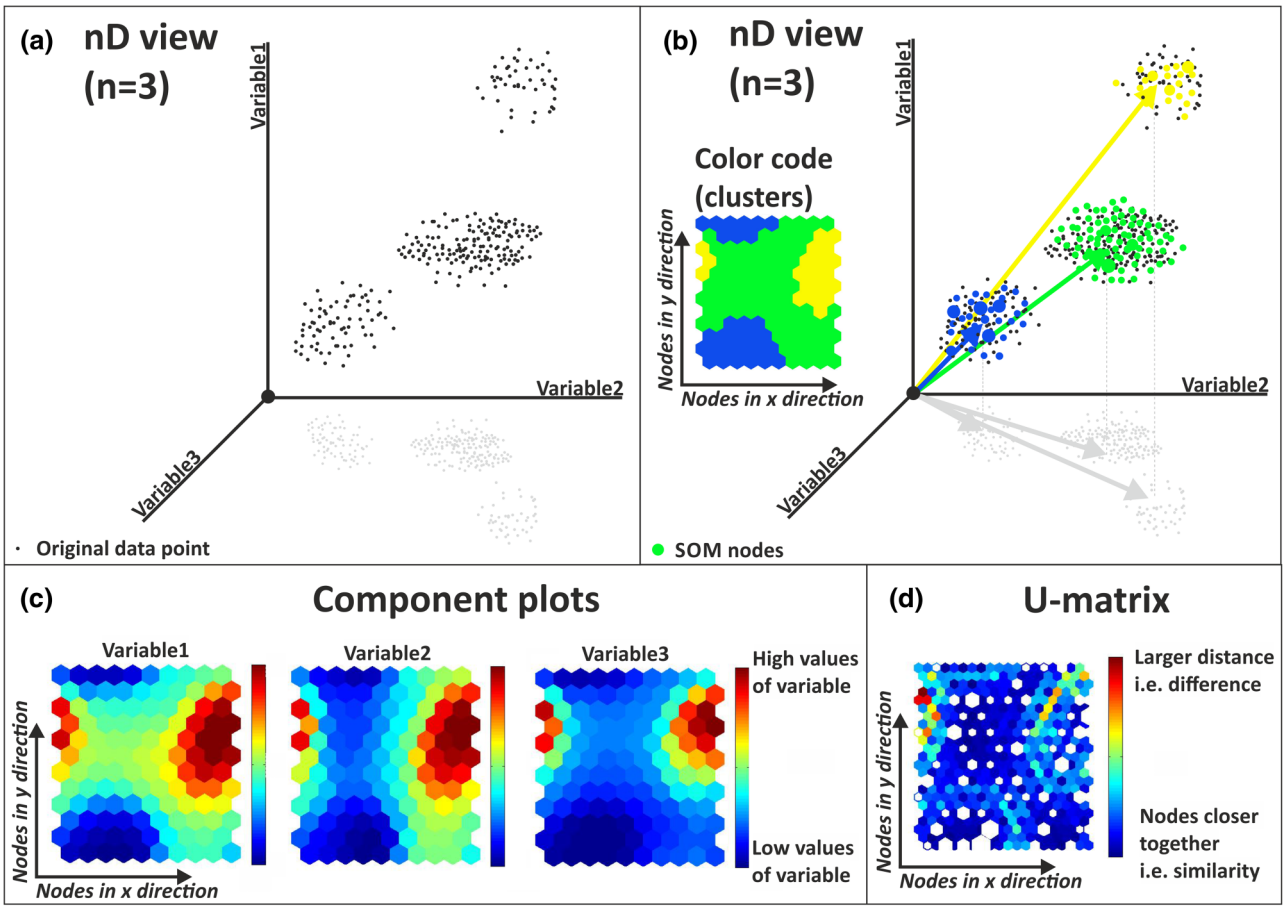

Figure 6 Principles and outputs of SOM: (a) nD view of the original data (black dots; three variables, i.e., three dimensions), and (b) SOM nodes representing that original data in yellow, green and blue dots (three clusters defined within the data). The outputs of SOM are presented in (c) component plots for each variable, and (d) the unified distance matrix (U-matrix) of the data. The component plot represents each node's contribution to a particular variable with smaller values of the variable in blue and larger in red. The U-matrix represents the distance between neighbouring nodes with blue colours indicating shorter distances, or similarity, and red colours larger distances, or difference. The white hexagons correspond to the number of original data samples within the node – the bigger the hexagon the more input samples fall within it. 'Empty' nodes are added in between the actual nodes to aid the visualization.

of SOM to predict seismic velocities from other available borehole data. The set of variables used in this study was selected based on the SOM analyses presented by Junno *et al.* (2019). In total, seven geophysical and geotechnical variables and nine geochemical variables were chosen for the final SOM analysis (Table 4). P-wave velocity (*Vp*), S-wave velocity (*Vs*), specific gravity (SG) and rock quality designation were included as direct indicators of properties controlling the reflectivity, and magnetic susceptibility, electrical resistivity and induced polarization effect as indicators of mineralization. Gamma–gamma density logs would have been available for 16 of the boreholes, but SG was chosen over gamma–gamma density as it reflects the same property but is more extensively measured, and based on the preliminary analyses it was found that SG actually correlates better with the seismic velocities. Geochemical variables selected were nickel (Ni), copper (Cu), gold (Au), palladium (Pd), platinum (Pt), iron (Fe), sulphur (S), cobalt (Co) and chromium (Cr) (Table 4). These are the primary constituents of the main sulphide minerals at Kevitsa (pyrrhotite, pentlandite, chalcopyrite and several platinum group minerals) and were included to differentiate mineralization from host rock signatures. Aluminium (Al), calcium (Ca), magnesium (Mg) and sodium (Na) could have been used as indicators of the magmatic layering and alteration; high Ca and Na concentrations are proxies for alteration, whereas high Mg concentrations relate to olivine pyroxenite and high Al to plagioclase-bearing olivine websterite. However, since Al, Ca, Mg and Na have been measured only very sporadically

Table 4 List of the SOM variables originally selected for the analysis. Also listed is the number of samples containing that particular variable and in how many different boreholes these samples exist. In total, there were 64,999 samples from 134 different boreholes. Only samples that contain at least one geophysical variable are included in the analysis

Variables	Unit	No. of Samples Containing that Variable	No. of Boreholes	Missing Percentage
Geophysical and geotechnical				
Vp	m/s	12,004	16	81.50
Vs	m/s	9878	14	84.80
Specific gravity (SG)	kg/m^3	46,611	105	28.30
Electrical resistivity	Ohm·m	31,627	60	51.30
IP	pct	31,021	59	52.30
RQD	pct	8113	13	87.50
Magnetic susceptibility	10×10^{-3} SI	7890	13	87.90
Geochemical				
Ni	pct	57,924	132	10.90
Cu	pct	57,921	132	10.90
Au	ppb	43,969	132	32.40
Pd	ppb	42,853	131	34.10
Pt	ppb	34,465	124	47.00
Fe	pct	57,924	132	10.90
S	pct	57,907	132	10.90
Co	ppm	57,924	132	10.90
Cr	ppm	57,924	132	10.90
Al	pct	17,142	45	73.60
Ca	pct	17,142	45	73.60
Mg	pct	17,142	45	73.60
Na	pct	17,142	45	73.60
Lithological labels		64,541	134	0.70
Alteration labels		26,982	134	58.50
Total		64,999	134	

(Table 4) and from different holes than most of the geophysical variables, they were, after initial testing, left out from the final SOM analysis.

After the SOM analysis, the lithology and alteration labels were checked for each cluster, the results of which are shown in the confusion matrices of Tables 6 and 7, respectively. For this purpose, the lithological classification was simplified (Table 1). The main focus of this work is on the intrusive rocks (olivine pyroxenite variants including also metaperidotite, and gabbro and olivine gabbro) and their relationship to the reflectivity properties, so the original classes for these rock types were respected (about 90% of all lithology labels fell into these groups). The dunite occurrences, about 4% of the lithology labels, were subdivided into three different groups: the Central Dunite, consisting of dunite and peridotite situated within the Central Dunite (Fig. 1); the Footwall Dunite consisting of dunite described at the basal contact of the intrusion; and the remaining dunite situated within the main Kevitsa intrusion (e.g. Standing *et al.* 2009; Gregory *et al.* 2011). Host rocks were subdivided into metavolcanics and metasediments that have similar petrophysical properties; this simplified 56 host rock classes into just two classes (in total only about 2.5% of all lithology labels were host rocks). Other rock groups, 1.5% of all lithology labels, include dykes, veins and xenoliths. Sulphide veins and fracture zones (1.3% of all lithology labels) were left as their own groups. About 0.7% of the selected samples had no lithology label logged for them. For the alteration labels, the original classification was respected (there were 11 different classes of alteration logged for the selected samples; Table 7). Alteration had been logged for 41.5% of the samples chosen for the analyses. Amphibole and serpentinite were the most common alteration types (about 82% of all the alteration labels were amphibole and 4% serpentinite). However, it should again be noted that amphibole alteration has been partly, but not consistently, also logged as metaperidotite in the lithology field rather than in the alteration field. Metaperidotite refers to amphibole-altered (in various degrees) olivine pyroxenite variants.

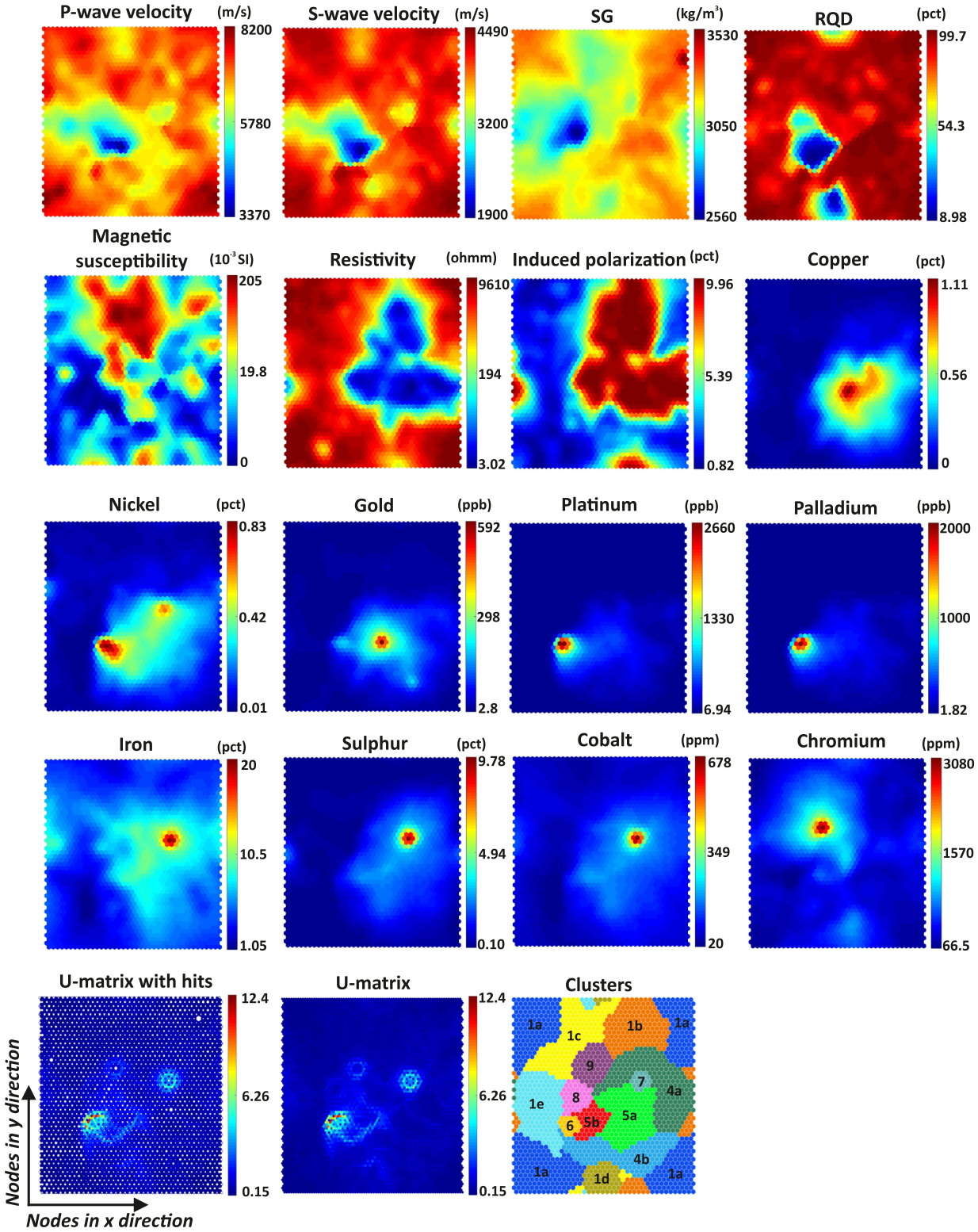

Figure 7 Selected component plots for different geophysical, geotechnical and geochemical variables. Thirteen clusters were defined within the data, including five clusters defining the barren olivine pyroxenites (clusters 1a, 1b, 1c, 1d and 1e), two clusters defining the transitional ore (clusters 4a and 4b), two clusters for regular ore (clusters 5a and 5b), and one cluster for the high Ni–PGE ore (cluster 6).

Lithological and alteration labels, which refer to descriptive drill hole loggings of lithology and alteration, were not included into the actual SOM analysis since based on extensive preliminary analyses and also according to paper by Junno *et al.* (2019), labels added uncertainty to the interpretation, and therefore, geophysical, geotechnical and geochemical, that is continuous physical variables, were considered to give more reliable results.

5 RESULTS

We present results for a Self-Organizing Map (SOM) run consisting of above-mentioned geophysical, geotechnical and geochemical variables. After initial testing, a toroid SOM map and an SOM size of 48 × 40 were chosen. The SOM model presented here has an average quantization error of 0.70 and topological error of 0.12. A Davies–Bouldin analysis suggested a local minimum at 13 clusters, which was chosen for further interpretation. The SOM results are interpreted based on the theoretical modelling presented in Section 3.1. The lithology and alteration labels for each cluster were checked after the SOM run and are presented in the confusion matrices shown in Tables 6 and 7, respectively.

5.1 The cause of reflectivity within the Kevitsa intrusion

The component plots for the Self-Organizing Map (SOM) run are shown in Fig. 7. Altogether 13 clusters were defined within the data, including five clusters interpreted as barren olivine pyroxenites (clusters 1a, 1b, 1c, 1d and 1e; Table 5), and four clusters for mineralization (clusters 4a, 4b, 5a and 5b; Table 5). The lithology and alteration were checked for these clusters after the analysis (Tables 6 and 7, respectively). Clusters 1a, 1b, 1c, 1d and 1e correspond to different olivine pyroxenite variants, whereas clusters 4a, 4b, 5a and 5b correspond mainly to olivine pyroxenite (Table 6). Clusters 5a and 5b are associated with the highest Ni and Cu concentrations, as well as low electrical resistivity and high induced polarization (IP) effect (Table 5 and Fig. 7). Cluster 5b is associated with low rock quality designation and, thus, the lowest seismic velocity and density values (Fig. 7 and Table 5). Clusters 4a and 4b are associated with medium Ni and Cu concentrations. Cluster 4a relates to low electrical resistivity and high IP effect, whereas cluster 4b relates to high electrical resistivity and low IP effect. Clusters 4a and 4b relate to higher seismic velocity than that of clusters 5a and 5b (Fig. 8). Cluster 4a and 4b are interpreted to represent *transitional ore*, and clusters 5a and 5b are interpreted to represent *regular ore*. These ore

Table 5 Average P-wave velocities and specific gravity (SG; i.e. density) for different clusters defined within the data based on the SOM analysis. Also shown are the calculated average acoustic impedance, and Ni, Cu, Au, Pt and Pd concentrations. Original data samples within the clusters are calculated. Last column presents the interpretation for what each cluster represents

Cluster	*Vp* (m/s)	SG (kg/m^3)	Impedance (10^6 kg/m^2/s)	RQD (pct)	Ni (pct)	Cu (pct)	Au (ppb)	Pt (ppb)	Pd (ppb)	*N*	Interpretation
1a	7396	3229	24	96	0.06	0.05	13	31	16	21,852	Olivine pyroxenites (barren; unaltered)
1b	7014	3160	22	94	0.07	0.06	18	37	22	7367	Olivine pyroxenites (barren; altered)
1c	6819	3098	21	90	0.05	0.03	11	29	14	6717	Olivine pyroxenites (barren; altered)
1d	6643	3096	21	41	0.11	0.07	26	77	49	2178	Olivine pyroxenites (barren; altered) and low RQD
1e	6192	2993	19	88	0.04	0.03	13	44	28	6478	Olivine pyroxenites (barren; altered)
4a	6847	3188	22	94	0.18	0.28	54	91	61	6416	Transitional ore
4b	6776	3184	22	92	0.26	0.30	99	244	162	4288	Transitional ore
5a	6479	3220	21	95	0.36	0.66	182	298	192	4755	Regular ore
5b	5022	3110	16	25	0.44	0.44	196	524	364	1097	Regular ore and low RQD
6	5462	3042	17	30	0.53	0.11	135	1646	1206	289	Ni-PGE, Host and low RQD
7	6275	3156	20	84	0.35	0.38	48	95	94	241	Veins, dykes and olivine pyroxenites ('False ore')
8	5400	2740	15	51	0.13	0.08	39	92	62	1538	Central Dunite and low RQD
9	7041	3031	21	93	0.09	0.06	20	41	26	1783	Host and olivine pyroxenites (barren; altered)

Table 6 Confusion matrix showing the percentage of different lithological groups within each cluster identified from the data

	Lithological Group	Cluster 1a	Cluster 1b	Cluster 1c	Cluster 1d	Cluster 1e	Cluster 4a	Cluster 4b	Cluster 5a	Cluster 5b	Cluster 6	Cluster 7	Cluster 8	Cluster 9
Olivine pyroxenite variants (OLPXs)	Olivine pyroxenite	59.59	49.25	35.09	45.45	25.13	56.87	68.33	71.69	67.09	48.44	17.84	13.33	30.85
	Olivine websterite	21.74	22.00	15.35	9.04	14.19	6.98	2.96	0.84	0.36	2.08	9.96	4.29	7.63
	Plag.-bearing olivine websterite	2.11	0.68	0.92	0.32	3.60	0.33	0.05	0.00	0.00	0.35	0.41	0.00	0.06
	Pyroxenite	1.29	0.30	0.73	0.32	3.54	0.03	0.61	0.29	0.00	0.00	0.00	2.60	1.79
	Websterite	0.60	0.30	0.95	1.97	4.82	0.26	0.68	0.00	1.64	1.04	0.41	2.93	0.11
	Metaperidotite	7.75	20.50	42.25	38.15	24.70	26.96	24.70	19.31	19.14	21.11	54.77	14.76	36.12
	Total OLPXs	93.08	93.02	95.30	95.27	75.96	91.44	97.32	92.13	88.24	73.01	83.40	37.91	76.56
Other lithological groups	Central Dunite	2.21	2.05	1.16	0.46	1.17	0.42	0.02	0.76	3.37	0.00	0.00	39.79	5.72
	Footwall Dunite	0.27	0.50	0.04	0.00	0.05	0.03	0.00	0.00	0.00	0.00	0.00	0.07	0.50
	Dunite	0.22	1.44	0.28	1.19	2.05	2.77	0.98	2.73	0.36	0.35	0.00	1.76	1.51
	Gabbros	0.73	0.46	0.89	0.73	6.58	0.31	0.44	0.15	2.10	7.27	0.00	3.45	0.34
	Veins, dykes	0.97	0.90	1.15	0.96	3.89	0.55	0.12	0.48	0.27	5.54	8.30	2.41	1.29
	Host	2.10	0.53	0.61	1.10	8.69	2.54	0.30	0.11	0.27	10.38	5.81	9.88	12.68
	Other	0.43	1.10	0.57	0.28	1.61	1.93	0.82	3.64	5.38	3.46	2.49	4.75	1.40
		100.00	100.00	100.00	100.00	100.00	100.00	100.00	100.00	100.00	100.00	100.00	100.00	100.00

Plag., plagioclase.

Table 7 Confusion matrix showing the percentage of different alteration labels within each cluster identified from the data

Alteration	Cluster 1a	Cluster 1b	Cluster 1c	Cluster 1d	Cluster 1e	Cluster 4a	Cluster 4b	Cluster 5a	Cluster 5b	Cluster 6	Cluster 7	Cluster 8	Cluster 9
Amphibolitic	38.52	44.25	48.58	34.80	44.58	26.90	22.29	18.68	16.59	13.49	29.46	23.67	48.35
No alteration label	57.37	53.36	48.47	62.21	47.02	69.89	76.73	80.44	79.03	82.70	61.83	32.38	30.34
Carbonate	0.12	0.24	1.58	1.38	1.76	0.87	0.35	0.38	0.46	0.00	6.64	1.24	2.69
Chloritic	0.04	0.03	0.15	0.23	0.56	0.31	0.02	0.27	0.18	0.00	0.41	2.15	0.56
Serpentinitic	1.82	1.66	0.54	0.32	0.68	1.37	0.14	0.11	3.37	0.00	0.00	35.50	5.78
Actinolitic	0.38	0.04	0.33	0.60	1.36	0.02	0.05	0.00	0.00	0.35	0.00	1.37	1.40
Albitic	0.14	0.03	0.01	0.05	0.97	0.41	0.00	0.06	0.00	0.00	0.00	1.89	2.36
Siliceous	1.24	0.00	0.04	0.00	0.42	0.11	0.00	0.06	0.00	0.00	1.24	0.39	1.79
Biotite	0.24	0.00	0.03	0.18	1.81	0.12	0.00	0.00	0.00	2.08	0.41	0.59	0.22
Tacl-carbonate	0.01	0.37	0.27	0.00	0.40	0.00	0.00	0.00	0.00	0.00	0.00	0.00	0.06
Epidote	0.08	0.03	0.00	0.14	0.40	0.00	0.40	0.00	0.36	1.38	0.00	0.00	0.00
Talc	0.02	0.00	0.00	0.09	0.05	0.00	0.02	0.00	0.00	0.00	0.00	0.85	6.45
	100.00	100.00	100.00	100.00	100.00	100.00	100.00	100.00	100.00	100.00	100.00	100.00	100.00

, *Geophysical Prospecting*, **68**, 82–102

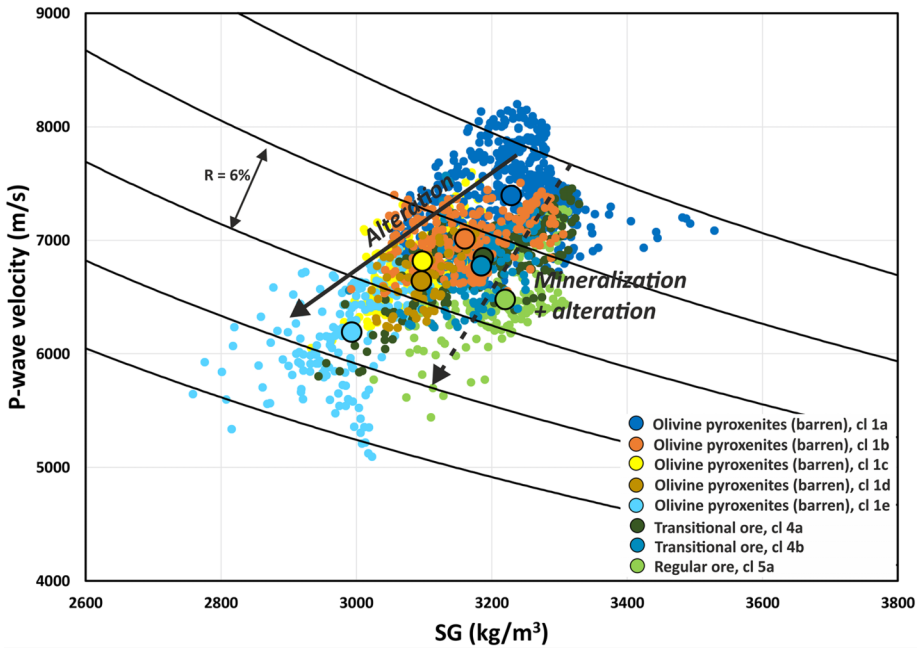

Figure 8 P-wave velocity versus density (SG) for the different clusters defined in Fig. 7. The solid black curves correspond to constant acoustic impedance, and the difference between two curves represents a detectable reflection (reflection coefficient equal to 6%; Salisbury *et al.* 1996; Salisbury *et al.* 2003). The black solid and dashed arrows show the effect of alteration and the combined effect of alteration and sulphide mineralization, respectively, based on modelling of reflectivity properties discussed in Section 3.1.

classes are similar to the division suggested by Mutanen (1997) and Gregory *et al.* (2011). The barren olivine pyroxenites divide into five clusters (clusters 1a, 1b, 1c, 1d and 1e; Fig. 7). The seismic velocity and density decreases from cluster 1a to clusters 1b, 1c, 1d and 1e with highest seismic velocity and density values associated with cluster 1a (Fig. 8). The percentage of metaperidotite, that is amphibole-altered olivine pyroxenites, increases from cluster 1a and 1b to clusters 1c, 1d and 1e (Table 6), that is lower seismic velocities seem to be associated with alteration (see Section 3.1). This is also evident in Table 7, where the percentage of logged amphibole alteration is higher for clusters 1b, 1c and 1e than for cluster 1a. However, it should be noted that the percentage for the 'no alteration label' is also high for these clusters. The lack of alteration label does not mean that the samples within these clusters are unaltered but simply indicates missing information on the alteration field. In addition, higher magnetic susceptibility, lower electrical resistivity and higher IP effect associated with clusters 1b, 1c and 1d are indicators of alteration. As evident in Fig. 8, unmineralized olivine pyroxenite (especially cluster 1a) is associated with higher seismic velocities than mineralized rock, but the density does not seem to differ much for the mineralized (clusters 4a, 4b and 5a) and barren (cluster 1a) clusters (Fig. 8). High Ni–PGE ore (cluster 6; Fig. 7) is also identified in the SOM run.

Figure 9 illustrates the three-dimensional (3D) spatial distribution of cluster 1a, representing unaltered, barren olivine pyroxenites, and cluster 1e, representing altered, barren olivine pyroxenites. These two clusters could produce an impedance contrast creating a reflection coefficient of about 13%. Most of the borehole data sit above 500 m depth, beneath which the observed continuous strong reflectivity in the 3D seismic data in Fig. 2 starts (Fig. 9). The two clusters with different average acoustic impedances alternate in the boreholes at these depths, and could cause the observed reflectivity. However, with the sparse borehole sampling, it is not possible to make definite conclusions about the continuity of the borehole layers with regard to the seismic data.

5.2 Other possible causes of reflectivity within and around the Kevitsa intrusion

In addition to alteration and mineralization, the other possible causes of reflectivity within the Kevitsa intrusion are the

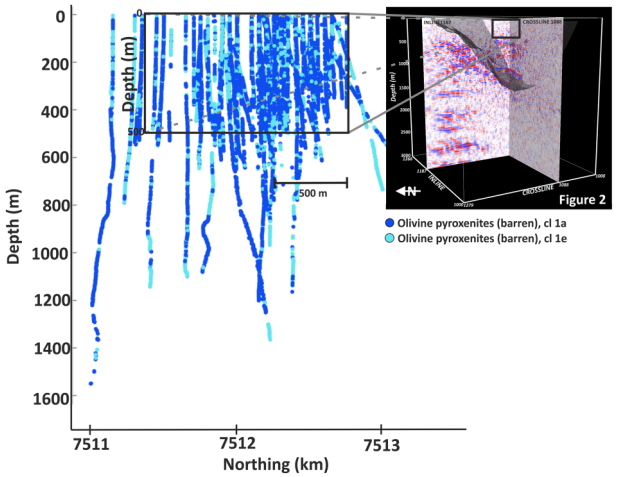

Figure 9 3D spatial distribution of cluster 1a, representing unaltered, barren olivine pyroxenite, and cluster 1e, representing altered, barren olivine pyroxenite. Most of the borehole data sit above the 500 m depth, beneath which the observed strong reflectivity in the 3D seismic data starts (Fig. 2). About 60 boreholes reach the depths of the observed reflectivity. These clusters alternate in the boreholes at these depths, and could be related to the cause of the observed reflectivity. Inset picture shows the approximate location of the samples with respect to the seismic cube (Fig. 2).

fracture and fault zones, dunite fragments and country rock occurrences internal to the intrusion, as well as dykes and veins. The fracture and fault zones and their expressions in the 3D seismic data have previously been extensively discussed by Malehmir *et al.* (2012b), Koivisto *et al.* (2015) and Lindqvist *et al.* (2017). Additionally, recently traveltime tomography using the first break picks of the Kevitsa three-dimesional (3D) seismic reflection data (Malehmir *et al.* 2018) provided an improved coverage at shallow depths, allowing a link between a major brittle structure observed in the 3D seismic data (Koivisto *et al.* 2015; Lindqvist *et al.* 2017) and surface observations. This structure is critical for mine planning and extends down to approximately 600 m with a lateral extent of more than 1000 m. However, fault and fracture zones, dunite fragments, country rock slabs or dykes and veins are not expected, at least based on the currently available data sets, to be the causes for the continuous, nearly horizontal reflections observed in the 3D seismic reflection data.

The Footwall Dunite unit is associated with high seismic velocity and density (Table 1). It is clearly visible in the 3D seismic reflection data and forms a lens like body at the basal contact of the intrusion (Koivisto *et al.* 2015). Low velocities and densities are associated with the thoroughly serpentinized Central Dunite (cluster 8; Table 5), which is clearly identifiable in the 3D seismic reflection data (Koivisto *et al.* 2015). The host rocks of the intrusion (metavolcanics and metasediments) are associated with the lowest seismic velocity and density values (clusters 6 and 9; Table 5) resulting in reflection coefficients of about 6–18% in contrast with barren olivine pyroxenites, and the basal contact of the intrusion to the host rocks is in fact the most prominent reflector in the area (Koivisto *et al.* 2012; Koivisto *et al.* 2015).

6 DISCUSSION AND CONCLUSIONS

The Self-Organizing Map (SOM) analysis of the Kevitsa borehole data, combined with theoretical modelling of the petrophysical properties of the Kevitsa rock types and ore, provides new insights into the origin of the observed reflectivity within the Kevitsa intrusion, and into its relationship to the Kevitsa disseminated sulphide mineralization. Koivisto *et al.* (2012), Koivisto *et al.* (2015) and Malehmir *et al.* (2012b, 2014) have previously suggested that contacts between the plagioclase-bearing olivine websterite tops and olivine pyroxenite bottoms (with increased sulphide mineralization) of smaller scale, internally differentiated magma layers might be the cause of reflections within the Kevitsa resource area. However, this interpretation is not unequivocally supported by the borehole data (Koivisto *et al.* 2015), since only little plagioclase-bearing olivine websterite is logged from the borehole data to trace such continuous lithological contacts (Gregory *et al.* 2011; Le Vaillant *et al.* 2016; Luolavirta *et al.* 2018a). Our current study similarly does not support that earlier interpretation.

The theoretical modelling of the effect of sulphide mineralization and alteration on the reflectivity properties of the Kevitsa rock types and ore (Fig. 5) suggests that the disseminated sulphide mineralization alone is not enough to produce reflections, but combining mineralization with the effect of alteration (amphibole and serpentinite) could produce observable reflections when in contact with unaltered and unmineralized zones. However, alteration products play the main role in determining the reflectivity characteristics of the olivine pyroxenite variants of the Kevitsa intrusion, and hence, altered, but unmineralized olivine pyroxenites in contact with unaltered, unmineralized olivine pyroxenites may also produce prominent reflections in the area.

The SOM results indicate that the regular ore zones are associated with lower seismic velocities and can be reflective when in contact with unmineralized and unaltered olivine pyroxenites (Fig. 8). Furthermore, the SOM results indicate that the mineralized zones are associated with alteration, which is, according to the theoretical calculations, needed in order to

produce detectable reflections. Since, the main mineralization (i.e. the regular ore) in Kevitsa occurs as continuous bodies extending up to hundreds of meters in diameter (Mutanen 1997), altered and mineralized zones could be the cause of observed reflectivity beneath the known deposit. Due to poor data quality at shallow depths, the 3D seismic data does not show any reflectivity at the depths of the known deposit. Nevertheless, we argue that the deeper, horizontal to gently dipping reflections are potential exploration targets in the area. It should, however, be noted again that the SOM results also indicate that unmineralized but altered olivine pyroxenites in contact with unmineralized and unaltered olivine pyroxenites could be the cause of reflections in the seismic data (Figs 8 and 9).

The origin of sulphur in the Kevitsa ore has been attributed to host rock contamination which took place by incorporation of metasedimentary material in the ultramafic magma (Mutanen 1997; Standing *et al.* 2009). Adding sulphur to the magma would have facilitated the crystallization of Ni and Cu in the sulphide phase instead of the silicate phase. Host rock contamination is also supported by the presence of graphite as the metasedimentary host rocks are (partly) sulphide-bearing carbonaceous black schists. In the case of host rock contamination, volatile components (S, C, H_2O, Cl), as well as other elements typical for metasediments (e.g. Al, Na, K and Si), would have been mixed in the crystallizing magma. Traces of these are reported by Mutanen (1997). Water provided by the host rock contamination is a necessary component in the alteration reactions, and it is feasible to think that the alteration started immediately after crystallization of the mafic minerals and continued until relatively low temperatures. The contamination model predicts that the ore mineral content should correlate with alteration.

According to Mutanen (1997), the main part of the intrusion was only marginally affected by contaminants and evolved autonomously. Here we pay attention to the observation by Standing *et al.* (2009) that compositional heterogeneity and variation, interpreted as smaller scale magmatic layering, could not be detected outside the Kevitsa resource area and, further, that the horizontal to gently dipping reflections are constrained mainly to the Kevitsa resource area (Koivisto *et al.* 2015). Therefore, a plausible hypothesis is that the formation of the ore deposit was controlled by the availability of contaminants and, where available, crystallization of the metals took place in the sulphide phase, and the ambient magmatic rock was also altered accordingly. The model allows for cyclic intrusions of several pulses of magma, but the final composition and mineralization would have depended on the availability of sulphur, volatiles and other contaminants from the host rock. As a result, the reflectivity would be a useful proxy for the mineralized and altered rocks in a less-altered environment.

Interpreting the deeper reflections observed in the 3D seismic data as altered and possibly mineralized zones would require that the mineralized and altered zones are somehow layered. Such a layering would be a natural result of adding cyclic, contaminated magma pulses to the intrusion. Thus, the observed reflectivity might originate from the altered pulses that could be associated with higher sulphide content (although this is not seismically required) in contact with less-altered unmineralized parts of the intrusion. However, as currently there is no understanding of the detailed distribution of alteration within the Kevitsa resource area, future work is required to further understand the relationship between the mineralization and alteration in detail.

ACKNOWLEDGEMENTS

This research is funded through a grant from K. H. Renlund Foundation to the first author. The authors would like to thank First Quantum Minerals Ltd. and Boliden for their collaboration and the data, and J. Kalla for the helpful comments. Paradigm GOCAD and Mira Geoscience Ltd. GOCAD Mining Suite provided an academic license used for 3D visualization of the seismic data. The SOM analysis was done using CSIRO's SiroSOM software. We acknowledge constructive comments provided by E. Schetselaar and anonymous reviewers along with the associate editor G. Bellefleur, which greatly helped to improve the quality of our work. Finally, we would like to acknowledge and thank S. Fraser for introducing us to the magical world of SOM. The idea for this study was innovated at an SOM course given by Stephen Fraser and held at the University of Helsinki. The authors declare no conflict of interest. The data that support the findings of this study are available from the corresponding author upon reasonable request. Partly, the data are subject to third party restrictions.

ORCID


N. Junno https://orcid.org/0000-0002-6802-5699

REFERENCES

Abers G.A. and Hacker B.R. 2016. A MATLAB toolbox and Excel workbook for calculating the densities, seismic wave speeds, major element composition of minerals and host rocks at pressure and temperature. *Geochemistry, Geophysics, Geosystems* **17**, 616–624.

Bass J.D. 1995. Elasticity of minerals, glasses and melts. In: *Mineral Physics and Crystallography: A Handbook of Physical Constants* (ed. T.J. Ahrens), pp. 45–63. American Geophysical Union.

Bierlein F.P., Fraser S.J., Brown W.M. and Lees T. 2008. Advanced methodologies for the analysis of databases of mineral deposits and major faults. *Australian Journal of Earth Sciences* **55**, 79–99.

Buske S., Bellefleur G. and Malehmir A. 2015. Introduction to special issues on "hard rock seismic imaging". *Geophysical Prospecting* **63**, 751–753.

Cottrell M. and Letrémy P. 2005. Missing values: processing with the Kohonen algorithm. Applied Stochastic Models and Data Analysis (ASMDA 2005) Proceedings, Brest, France, May 2005, pp. 489–496.

Cracknell M.J., Reading A.M. and McNeill A.W. 2014. Mapping geology and volcanic-hosted massive sulphide alteration in the Helley-Mt Charter region, Tasmania, using Random Forests and Self-Organizing Maps. *Australian Journal of Earth Sciences* **61**, 287–304.

Davies D.L. and Bouldin D.W. 1979. A cluster separation measure. *IEEE Transactions on Pattern Analysis and Machine Intelligence* **PAMI-1**, 224–227.

Eaton D., Milkereit B. and Salisbury M. 2003. Seismic methods for deep mineral exploration: mature technologies adapted to new targets. *The Leading Edge* **22**, 580–585.

Fessant F. and Midenet S. 2002. Self-organising map for data imputation and correction in surveys. *Neural Computing & Applications* **10**, 300–310.

Fraser S. and Dickson B.L. 2007. A new method for data integration and integrated data interpretation: self-organizing maps. *Proceedings of Exploration 07: 5th Decennial International Conference on Mineral Exploration*, Toronto, Canada, September 2007, pp. 907–910.

Gregory J., Journet N., White G. and Lappalainen M. 2011. *Kevitsa Nickel Copper Project, Finland*. Technical Report (NI 43–101) for the Mineral Resources and Reserves of the Kevitsa Project. First Quantum Minerals Ltd.

Heinonen S., Imaña M., Snyder D.B., Kukkonen I.T. and Heikkinen P.J. 2012. Seismic reflection profiling of the Pyhäsalmi VHMS-deposit: a complementary approach to the deep base metal exploration in Finland. *Geophysics* **77**, WC15–WC23.

Horrocks T.A. 2019. Integrated analysis of geological, geophysical, and geochemical data of the Kevitsa Ni-Cu-PGE deposit: machine learning approaches. PhD thesis, School of Earth Sciences, University of Western Australia, Australia.

Junno N., Koivisto E., Kukkonen I., Malehmir A. and Montonen M. 2019. Predicting missing seismic velocity values using self-organizing maps to aid the interpretation of seismic reflection data from the Kevitsa Ni-Cu-PGE deposit in northern Finland. *Minerals* **9**, 529.

Kaski S., Kangas J. and Kohonen T. 1998. Bibliography of Self-Organizing Map (SOM) papers: 1981–1997. *Neural Computing Surveys* **1**, 1–176.

Kieu D.T., Kepic A. and Kitzig M.C. 2018. Prediction of sonic velocities from other borehole data: An example from the Kevitsa mine site, northern Finland. *Geophysical Prospecting* **66**, 1667–1683.

Klose C.D. 2006. Self-organizing maps for geoscientific data analysis: geological interpretation of multidimensional geophysical data. *Computational Geosciences* **10**, 265–277.

Kohonen T. 1981. Automatic formation of topological maps of patterns in a self-organizing system. *Proceedings of the Second Scandinavian Conference on Image Analysis*, Helsinki, Finland, June 15–17, 1981, pp. 214–220.

Kohonen T. 2001. *Self-Organizing Maps*. Springer, New York, NY.

Kohonen T., Hynninen J., Kangas J. and Laaksonen J. 1996. *SOM_PAK: the self-organizing map program package*. Technical Report A31, Laboratory of Computer and Information Science, Helsinki University of Technology.

Koivisto E., Malehmir A., Heikkinen P., Heinonen S. and Kukkonen I. 2012. 2D seismic reflection investigations at the Kevitsa Ni-Cu-PGE deposit, northern Finland. *Geophysics* **77**, WC149–WC162.

Koivisto E., Malehmir A., Hellqvist N., Voipio T. and Wijns C. 2015. Building a 3D model of lithological contacts and near-mine structures in the Kevitsa mining and exploration site, northern Finland. *Geophysical Prospecting* **63**, 754–773.

Kokko S. 2018. *Mineral resources and mineral reserves, 2018*. Boliden Summary Report.

Kukkonen I., Lahti I., Heikkinen P. and HIRE Working Group of the Geological Survey of Finland. 2009. *HIRE Seismic Reflection Survey in the Kevitsa Ni-PGE deposit, North Finland*. Geological Survey of Finland Report Q23/2008/59.

L'Heureux E., Milkereit B. and Vasudevan K. 2009. Heterogeneity and seismic scattering in exploration environments. *Tectonophysics* **472**, 264–272.

Le Vaillant M., Barnes S.J., Fiorentini M.L., Santaguida F. and Törmänen T. 2016. Effects of hydrous alteration on the distribution of base metals and platinum group elements within the Kevitsa magmatic nickel sulphide deposit. *Ore Geology Reviews* **72**, 128–148.

Leväniemi H., Hulkki H. and Tiainen M. 2016. SOM guided fuzzy logic prospectivity model for gold in the Häme Belt, southwestern Finland. *Journal of African Earth Sciences* **128**, 72–83.

Lindqvist T., Skyttä P., Koivisto E.A.-L., Häkkinen T. and Somervuori P. 2017. Delineating the network of brittle structures with geotechnical, structural and reflection seismic data, Kevitsa open pit, northern Finland, *GeoResJ* **13**, 159–174.

Luolavirta K., Hanski E., Maier W. and Santaguida F. 2018a. Whole-rock and mineral compositional constraints on the magmatic evolution of the Ni-Cu-(PGE) sulfide ore-bearing Kevitsa intrusion, northern Finland. *Lithos* **269–299**, 37–53.

Luolavirta K., Hanski E., Maier W., Lahaye Y., O'Brien H. and Santaguida F. 2018b. In situ strontium and sulfur isotope investigation of the Ni-Cu-(PGE) sulfide ore-bearing Kevitsa intrusion, northern Finland. *Mineralium Deposita* **53**, 1019–1038.

Luolavirta K., Hanski E., Maier W. and Santaguida F. 2018c. Characterization and origin of dunitic rocks in the Ni-Cu sulphide-bearing Kevitsa intrusion: whole-rock and mineral compositional constrains. *Bulletin of the Geological Society of Finland* **90**, 5–32.

Malehmir A., Durrheim R., Bellefleur G., Urosevic M., Juhlin C., White D.J. *et al.* 2012a. Seismic methods in mineral exploration and mine planning: a general overview of past and present case histories and a look into the future. *Geophysics* **77**, WC173–WC190.

Malehmir A., Juhlin C., Wijns C., Urosevic M., Valasti P. and Koivisto E. 2012b. 3D seismic reflection imaging for open-pit mine planning and deep exploration in the Kevitsa Ni-Cu- PGE deposit, northern Finland. *Geophysics* **77**, WC95–WC108.

Malehmir A., Koivisto E., Manzi M., Cheraghi S., Durrheim R.J., Bellefleur G. *et al.* 2014. A review of seismic reflection investigations in three major metallogenic regions: the Kevitsa Ni-Cu-PGE (Finland), Witwatersrand goldfields (South Africa), and the Bathurst Mining Camp (Canada). *Ore Geology Reviews* **56**, 423–441.

Malehmir A., Bellefleur G., Koivisto E. and Juhlin C. 2017. Pros and cons of 2D vs 3D seismic mineral exploration surveys. *First Break* **35**, 49–55.

Malehmir A., Tryggvason A., Wijns C., Koivisto E., Lindqvist T., Skyttä P. *et al.* 2018. Why 3D seismic data are an asset for both exploration and mine planning? Velocity tomography of weakness zones in the Kevitsa Ni-Cu-PGE mine, northern Finland. *Geophysics* **83**, B33–B46.

Milkereit B., Eaton D.W., Wu J., Perron G., Salisbury M.H., Berrer E. *et al.* 1996. Seismic imaging of massive sulphide deposits: Part II. Seismic reflection profiling. *Economic Geology* **91**, 829–834.

Mutanen T. 1997. *Geology and Ore Petrology of the Akanvaara and Koitelainen Mafic-Layered Intrusions and the Keivitsa-Satovaara Layered Complex, northern Finland*. Geologian Tutkimuskeskus, Espoo.

Mutanen T. and Huhma H. 2001. U-Pb geochronology of the Koitelainen, Akanvaara and Keivitsa mafic layered intrusions and related rocks. In: *Radiometric Age Determinations from Finnish Lapland and Their Bearing on the Timing of Precambrian Volcano-Sedimentary Sequences* (ed. M. Vaasjoki), pp. 229–246. Geological Survey of Finland.

Oja M., Kaski S. and Kohonen T. 2003. Bibliography of self-organizing map (SOM) papers: 1998–2001 addendum. *Neural Computing Surveys* **3**, 1–156.

Penn B.S. 2005. Using self-organizing maps to visualize high-dimensional data. *Computers & Geosciences* **31**, 531–544.

Pöllä M., Honkela T. and Kohonen T. 2009. Bibliography of self-organizing map (SOM) papers: 2002–2005 addendum. Technical Report TKK-ICS-R23, Helsinki University of Technology.

Salisbury M., Milkereit B. and Bleeker W. 1996. Seismic imaging of massive sulphide deposits: part I. Rock properties. *Economic Geology* **91**, 821–828.

Salisbury M., Harvey C.W. and Matthews L. 2003. The acoustic properties of ores and host rocks in hardrock terranes. In: *Hardrock Seismic Exploration* (eds D. Eaton, B. Milkereit and M. Salisbury), pp. 9–19. SEG.

Santaguida F., Luolavirta K., Lappalainen M., Ylinen J., Voipio T. and Jones S. 2015. The Kevitsa Ni-Cu-PGE deposit in the Central Lapland Greenstone Belt in Finland. In: *Mineral Deposits of Finland* (eds W.D. Maier, R. Lahtinen and H. O'Brien), pp. 195–210. Elsevier.

Standing J., De Luca K., Outhwhaite M., Lappalainen M., Wijns C., Jones S. *et al.* 2009. Report and recommendations from the Kevitsa Campaign, Finland. Confidential Report to First Quantum Minerals Ltd. Jigsaw Geosciences Pty Ltd., West Perth, Australia.

Steel M.A. 2011. Petrophysical modelling using self-organizing maps. Bachelor's thesis, Department of Exploration Geophysics, Curtin University of Technology, Australia.

Vesanto J., Himberg J., Alhoniemi E. and Parhankangas J. 2000. SOM Toolbox for Matlab 5. Technical Report A57, Laboratory of Computer and Information Science, Helsinki University of Technology.

Yang S.-H., Maier W.D., Hanski E., Lappalainen M., Santaguida F. and Määttä S. 2014. Origin of ultra-nickeliferous olivine in the Kevitsa Ni-Cu-PGE-mineralized intrusion, northern Finland. *Contributions to Mineralogy and Petrology* **166**, 81–95.

